HHS Public Access

Author manuscript

ACS Infect Dis. Author manuscript; available in PMC 2021 August 14.

Published in final edited form as:

ACS Infect Dis. 2020 August 14; 6(8): 2249–2259. doi:10.1021/acsinfecdis.0c00374.

Positron Emission Tomography Imaging of *Staphylococcus aureus* Infection Using a Nitro-Prodrug Analog of 2-[^{18}F]F-*p*-Aminobenzoic Acid

Yong Li[†,‡,£], **Fereidoon Daryaee**[†,‡,£], **Grace E. Yoon**[‡,⊥], **Doyoung Noh**[‡,⊥], **Peter M Smith-Jones**[⊥], **Yuanyuan Si**[‡], **Stephen G. Walker**[§], **Nashaat Turkman**[¶], **Labros Meimetis**[£], **Peter J. Tonge**[†,‡,¶,£,*]

[†]Center for Advanced Study of Drug Action, Stony Brook University, 100 Nicolls Road, 633 Chemistry, Stony Brook, New York 11794, United States

[‡]Department of Chemistry, Stony Brook University, 100 Nicolls Road, 633 Chemistry, Stony Brook, New York 11794, United States

[¶]Department of Radiology, Stony Brook University, 100 Nicolls Road, 633 Chemistry, Stony Brook, New York 11794, United States

[§]Department of Oral Biology and Pathology, Stony Brook University, Stony Brook, NY 11794-3400, United States

[⊥]The Facility for Experimental Radiopharmaceutical Manufacturing, Department of Psychiatry, Stony Brook University, Stony Brook, New York 11794, United States

[£]Chronus Pharmaceuticals, 25 Health Sciences Drive, Stony Brook, New York, 11790-3350, United States

Abstract

Deep seated bacterial infections caused by pathogens such as *Staphylococcus aureus* are difficult to diagnose and treat and are thus a major threat to human health. In previous work we demonstrated that positron emission tomography (PET) imaging with 2-[^{18}F]F-*p*-aminobenzoic acid (2-[^{18}F]F-PABA) could non-invasively identify, localize and monitor *S. aureus* infection with excellent sensitivity and specificity in a rodent soft tissue infection model. However, 2-[^{18}F]F-PABA is rapidly N-acetylated and eliminated, and in an attempt to improve radiotracer accumulation in bacteria we adopted a pro-drug strategy in which the acid was protected by an ester and the amine was replaced with a nitro group. Metabolite analysis indicated that the nitro group of ethyl 2-[^{18}F]fluoro-4-nitrobenzoate (2-[^{18}F]F-ENB) is converted to the corresponding amine by bacteria-specific nitroreductases while the ester is hydrolyzed *in vivo* into the acid.

[*]**Corresponding Author**: Tel.: (631) 632 7907. peter.tonge@stonybrook.edu.

The Supporting Information is available free of charge on the ACS Publications website at DOI:
The Supporting Information contains additional data regarding HPLC analysis of 2-[^{18}F]F-ENB and 2-[^{18}F]F-NB, cellular uptake of 2-[^{18}F]F-NB, histology of infected and inflamed tissues, *in vitro* metabolic stability of 2-[^{18}F]F-ENB, time activity curves and biodistribution for 2-[^{18}F]F-NB in major tissues, steady state kinetic data of 2-F-ENB, 2-F-NB and 2-F-NAP, and chemical characterization data for 2-F-ENB and 2-F-NAP.

CONFLICT OF INTEREST STATEMENT

The authors declare the following competing financial interest(s): P.J.T. is the cofounder of Chronus Pharmaceuticals Inc.

PET/CT imaging of 2-[^{18}F]F-ENB and the corresponding acid 2-[^{18}F]F-NB in a rat soft tissue infection model demonstrated colocalization of the radiotracer with the bioluminescent signal arising from *S. aureus* Xen29, and demonstrated that the tracer could differentiate *S. aureus* infection from sterile inflammation. Significantly, the accumulation of both 2-[^{18}F]F-ENB and 2-[^{18}F]F-NB at the site of infection was 17-fold higher than at the site of sterile inflammation compared to 8-fold difference observed for 2-[^{18}F]F-PABA, supporting the proposal that the active radiotracer *in vivo* is 2-[^{18}F]F-NB. Collectively, these data suggest that 2-[^{18}F]F-ENB and 2-[^{18}F]F-NB have the potential for translation to humans as a rapid, noninvasive diagnostic tool to identify and localize *S. aureus* infections.

Graphical Abstract

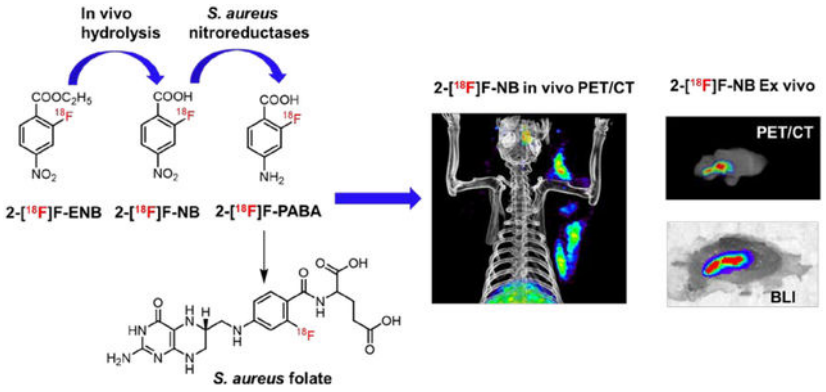

Keywords

PET imaging; deep-seated infection; non-invasive; *Staphylococcus aureus*; preclinical; folate

Deep-seated infections caused by the Gram-positive pathogen *Staphylococcus aureus*, such as infective endocarditis, prosthetic joint infections and osteomyelitis, are life-threatening diseases that are challenging to diagnose leading to substantial morbidity and mortality.[1] Current diagnostic methods for deep seated infections can be slow or inaccurate, and often rely on the availability of clinical samples that contain bacteria which are difficult to obtain. While the availability of non-invasive imaging methods such as X-ray, computed tomography (CT) and magnetic resonance imaging (MRI), have improved the ability to diagnose infection, these methods rely on the physiological changes caused by the bacterial infection, and thus their results can be confused by other clinical changes unrelated to infection such as inflammatory disorders. Therefore, a non-invasive, sensitive and bacteria-specific imaging tool is urgently needed to facilitate accurate diagnosis to better inform on clinical decision-making, leading to improved patient outcomes.

Nuclear medicine imaging modalities such as positron emission tomography (PET) and single-photon emission computed tomography (SPECT) are currently used clinically to detect and diagnose infectious diseases.[2,3] This includes PET imaging of [^{18}F]fluorodeoxyglucose ([^{18}F]FDG) or radiolabeled white blood cells (WBC).[4–6] Unfortunately, these approaches lack specificity since they primarily detect the inflammatory

response to infection. Therefore, to overcome this obstacle molecular imaging probes that directly target bacteria are highly desired. Recent efforts to develop bacteria specific and bacteria-class specific PET tracers are summarized in several detailed recent reviews.[7–9] In particular, the folate pathway is regarded as a promising imaging target to develop bacteria specific imaging tracers because folate must be biosynthesized by a wide range of bacteria. For example, ^{18}F-fluoropropyl-trimethoprim,[10] a ^{18}F analog of the bacterial dihydrofolate reductase (DHFR) inhibitor trimethoprim, and ^{11}C-*p*-aminobenzoic acid ([^{11}C]-PABA),[11] a ^{11}C-labeled dihydropteroate synthase (DHPS) substrate, have been explored as potential radiotracers for imaging Gram positive and Gram negative bacterial infections.

Previously our group successfully developed a bacteria-specific PET tracer, 2-[^{18}F]F-*p*-aminobenzoic acid (2-[^{18}F]F-PABA) to identify and localize *S. aureus* in a rodent soft tissue infection model.[12] *In vitro* enzymatic assays supported a mechanism for tracer accumulation in which bacterial dihydropteroate synthase (DHPS) catalyzes the incorporation of 2-[^{18}F]F-PABA into folate. However, *in vivo* metabolite analysis demonstrated that 2-[^{18}F]F-PABA underwent rapid N-acetylation, a transformation that would prevent the incorporation of the radiotracer into folic acid. To avoid N-acetylation, we replaced the aromatic amine with a nitro group based on the premise that bacteria contain nitroreductases that are more efficient at reducing aromatic nitro groups compared to those found in the liver.[13,14] A number of fluorescent, luminescent and MRI probes have also been developed using the activity of bacterial nitroreductases to reduce aromatic nitro functionality to the corresponding amine.[15–19] In addition, we posited that the rapid renal clearance of 2-[^{18}F]F-PABA was partly responsible for the relatively low absolute uptake of this tracer at the site of infection. Thus, to reduce renal clearance, we converted the carboxylate to the less polar ethyl ester.[20] A method for synthesizing ethyl 2-[^{18}F]F-4-nitrobenzoate (2-[^{18}F]F-ENB) in high radiochemical yield was developed and this second generation tracer together with the corresponding acid 2-[^{18}F]F-4-nitrobenzoate (2-[^{18}F]F-NB) were evaluated in a rat triceps infection model.

RESULTS

Synthesis of 2-[^{18}F]F-ENB

Ethyl 2-[^{18}F]F-4-nitrobenzoate (2-[^{18}F]F-ENB) was prepared via one-step manual radiosynthesis using ethyl 2,4-dinitro benzoate as the starting material (Figure 1A). The radioactive product was collected following HPLC and the identity of the radiotracer was confirmed by demonstrating that the retention time of the labeled material matched that of the cold reference standard ethyl 2-F-4-nitrobenzoate (2-F-ENB) (Figure S1 and S2a, b). The overall synthesis time was 90 min with a radiochemical yield (RCY) of 7% (n=8, decay-corrected). A primary factor in the moderate RCY of 2-[^{18}F]F-ENB was assumed to arise from the steric hindrance of the ortho ethyl ester group which directed the radio-fluorination preferentially to the para-position. The specific activity of 2-[^{18}F]F-ENB was calculated to be 3983 ± 1704 mCi/μmole using a standard curve based on the UV absorbance of 2-F-ENB at 287 nm, and the radiochemical purity was determined to be 99.2 ± 0.7 %. To improve the RCY of 2-[^{18}F]F-ENB and facilitate clinical translation, an automated three-step radiosynthesis method using 2,4-dinitro benzonitrile as an alternative precursor was also

developed (Figure 1B and Figure S2c, d). The total synthesis time of 2-[^{18}F]F-ENB was 90 min with a typical decay-corrected yield of 29%, and the final product had an average specific activity of 2556 mCi/μmole.

2-[^{18}F]F-ENB PET can distinguish infection from inflammation

The critical requirement for an ideal bacteria-specific tracer is its ability to distinguish active infection from sterile inflammation. Therefore, we developed a mixed infection and inflammation rat triceps model to evaluate 2-[^{18}F]F-ENB. The model was established by intramuscular injection of *S. aureus* into the right triceps and a 10-fold higher burden of heat-killed *S. aureus* into the left triceps to induce sterile inflammation. Tissue histology confirmed the presence of *S. aureus* in the infected triceps while no bacterial colonies were found in the contralateral triceps (Figure S3). The level of inflammation in both triceps was evaluated by [^{18}F]FDG, which is commonly used to assess the host inflammatory response. The radioactivity associated with [^{18}F]FDG in the infected and the inflamed triceps was similar (0.8% ID/cc and 1.2% ID/cc, respectively, p>0.05) (Figure 2A and 2B). The biodistribution of 2-[^{18}F]F-ENB was evaluated in this same model at 3 h post tracer administration showing that the ratio of radioactivity in the infected triceps to inflamed triceps was 17 (Figure 2C and 2D).

To further examine the biodistribution of the radiotracer in the infected and inflamed triceps, both triceps were excised following *in vivo* PET imaging and analyzed using *ex vivo* tissue PET imaging, bacterial culture and histology (Figures 2E, 2F, S3 and S4). This showed that the radioactive signal in the infected triceps co-localized with regions of *S. aureus* Newman infection.

2-[^{18}F]F-ENB-associated radioactivity colocalizes with *S. aureus* bioluminescence.

The bioluminescent *S. aureus* strain Xen29 has previously been used to monitor antibiotic efficacy using preclinical bioluminescence imaging,[21,22] and also as a complementary *in vivo* imaging modality.[23] Therefore, to confirm that the PET signal in the infected triceps was derived from *S. aureus*, the triceps infection was induced using *S. aureus* Xen29 for colocalization experiments. At 180 min post tracer injection, the radioactive signal was predominantly observed in the infected triceps, consistent with the imaging data for the Newman strain of *S. aureus* (Figure 3B). *Ex vivo* PET imaging further demonstrated the localization of radioactivity in the infected triceps, while *ex vivo* bioluminescence showed colocalization of the PET signal with signal arising from bioluminescence imaging (BLI) (Figure 3C).

2-[^{18}F]F-ENB is rapidly hydrolyzed to 2-[^{18}F]F-NB but the nitro group is metabolically stable

We analyzed the *in vitro* metabolic stability of 2-[^{18}F]F-ENB to assess the lability of the ester protecting group and the overall stability of the nitro group. We found that 2-[^{18}F]F-ENB was efficiently hydrolyzed in rat serum to the corresponding acid 2-[^{18}F]fluoro-4-nitrobenzoate (2-[^{18}F]F-NB) with a half-life of 2 min whereas the nitro group was unaffected over the 85-min incubation period (Figure S5a–e). A similar result was observed in human serum although the half-life for hydrolysis was 35 min (Figure S5f). We then

analyzed the stability of 2-[^{18}F]F-ENB in rat blood *in vivo*. After intravenous administration of 2-[^{18}F]F-ENB into healthy rats, blood samples were taken at 5, 30 and 60 min and analyzed by radio-HPLC which demonstrated that 2-[^{18}F]F-NB was the predominant radioactive component at each time point (Figure 4B). Analysis of urine samples at 30 and 60 min post injection also revealed that the majority of the radioactive signal could be attributed to 2-[^{18}F]F-NB (Figure 4C). Together, these data indicate that the ester is rapidly hydrolyzed but that the aromatic nitro group of 2-[^{18}F]F-ENB is metabolically stable *in vivo*. The *in vivo* studies also revealed small amounts of 2-[^{18}F]F-PABA and the N-acetylated analog of 2-[^{18}F]F-PABA in the blood and urine, and we note that both the liver and bacteria in the intestinal flora contain nitroreductases capable of reducing aromatic nitro groups.[13,14] Based on studies with 4-nitrobenzoic acid, it is likely that intestinal bacteria are the primary source of the nitroreductase activity.[13,14]

2-[^{18}F]F-NB is responsible for the radioactive signal at the site of infection

Due to the rapid hydrolysis of 2-[^{18}F]F-ENB to 2-[^{18}F]F-NB in plasma, we hypothesized that 2-[^{18}F]F-NB would be the active radiotracer responsible for the PET signal at the site of infection. To test this hypothesis, 2-[^{18}F]F-NB was radiosynthesized using a GE Tracerlab FXN Pro Radiosynthesis Module (Figure 5A and S6) and evaluated in the same infection model. At 3 h post injection, PET imaging results demonstrated that the radioactivity associated with 2-[^{18}F]F-NB was localized at the site of infection and also colocalized with the bioluminescence signal arising from *S. aureus* Xen29 (Figure 5B–D). Quantitative analysis of the ROI showed that the signal at the infection site was 17-fold higher than the one at the site of sterile inflammation, an observation supported by *ex vivo* gamma counting (Figure S7c and 7d).

2-F-ENB and 2-F-NB are substrates for *S. aureus* NfsB.

We hypothesized that the accumulation of radioactivity at the site of infection was partly due to the conversion of 2-[^{18}F]F-ENB into 2-[^{18}F]F-PABA which could then be potentially incorporated into folic acid. Above we demonstrated that 2-[^{18}F]F-ENB is rapidly hydrolyzed to 2-[^{18}F]F-NB, and that 2-[^{18}F]F-NB recapitulates the imaging results obtained with 2-[^{18}F]F-ENB. We next assessed the ability of the aromatic nitro group in 2-F-ENB and 2-F-NB to be reduced to the corresponding amine by the *S. aureus*-specific nitroreductase NfsB. *S. aureus* NfsB was cloned, expressed and purified, and F-ENB and F-NB were evaluated as substrates using NADH as the cofactor.[24] NfsB was found to efficiently reduce both 2-F-ENB and 2-F-NB, with k_{cat}/K_m values of 5.7×10^5 $M^{-1}s^{-1}$ and 1.8×10^4 $M^{-1}s^{-1}$, respectively (Table 1 and Figure S8). This differential activity of *S. aureus* NfsB towards the ester and acid was also observed for both the *Escherichia coli* nitroreductases NfsA and NfsB towards methyl 4-nitrobenzoate and 4-nitrobenzoate.[25] Thus, the data support the proposal that the *in vivo* signal at the site of infection could result from the conversion of the radiotracers into 2-[^{18}F]F-PABA which is a substrate for DHPS.

2-F-NB can antagonize the bacteriostatic effect of sulfonamide with *S. aureus* Xen29

F-PABA is a substrate for dihydropteroate synthase (DHPS) in the folate biosynthesis pathway, and to provide further evidence for the proposed mechanism of action (MOA) of our second generation tracers, we established a phenotypic assay to evaluate the ability of F-

PABA and F-NB to rescue the antibacterial effect of the DHPS inhibitor sulfamethoxazole (SMX). We first demonstrated that 2-[^{18}F]F-NB was taken up by both *S. aureus* Newman and Xen29. Time dependent uptake of 2-[^{18}F]F-NB was observed during the 120 min incubation period but not by heat killed bacteria, suggesting a specific uptake mechanism (Figure S9). We then validated the MOA assay with the endogenous DHPS substrate PABA, and showed that bacterial regrowth in the presence of sulfamethoxazole occurred upon the addition of PABA (Figure 6A). F-PABA also rescued bacterial growth in a concentration-dependent manner and it was shown that 0.8 and 4 μg/mL of F-PABA increased the minimum inhibitory concentration (MIC) of sulfamethoxazole by 8-fold (1.56 to 12.5 μg/mL) and to over 100 μg/mL, respectively (Figure 6B). Similarly, 2-F-NB also antagonized the activity of sulfamethoxazole, and 40 μg/mL 2-F-NB resulted in a shift in the sulfamethoxazole MIC from 1.56 μg/mL to 12.5 μg/mL (Figure 6C). In contrast, 2-fluoro-4-nitroacetophenone (2-F-NAP), a structural analog of FNB and also an efficient substrate for the *S. aureus* nitroreductase NfsB ($k_{cat}/K_m = 5.7\times10^5$ $M^{-1}s^{-1}$, Figure S8), was unable to rescue growth in the presence of sulfamethoxazole (Figure 6D). Furthermore, our previously established HPPK-DHPS-DHFR coupled assay demonstrated that 2-fluoro-4-aminoacetophenone was not an efficient substrate for DHPS even at a concentration of 80 μM, supporting the link between the folate pathway and the MOA of 2-F-NB.

DISCUSSION

Non-invasive imaging is a very promising approach for the detection and localization of deep-seated infections caused by pathogens such as *S. aureus*, and there are major ongoing efforts to develop molecular probes that selectively accumulate at the site of infection. Modalities that are being exploited include optical imaging based on fluorescent probes and nuclear imaging using radiotracers. Although bacteria-specific fluorescent probes have been used to detect *S. aureus* infection in animal models,[18,26,27] the clinical translation of these compounds may be impacted by absorption and scattering of light by tissue. Nuclear medicine imaging modalities such as PET and SPECT, on the other hand, have great clinical potential for infection diagnosis due to their superior sensitivity and ability of the radiation to penetrate tissue. Consequently, there are numerous efforts to develop bacteria-specific PET probes with the appropriate pharmacokinetic properties, and radiotracers that are currently being evaluated include ^{18}F-labeled maltohexaose (MH^{18}F),[28] 6-[^{18}F]-fluoromaltose,[29] 2-[^{18}F]F-fluorodeoxysorbitol,[30] 6-^{18}F-fluoromaltotriose,[31] [^{18}F]fluoropropyl-trimethoprim,[10] and [^{11}C]-D-amino acids.[32,33] Although the evaluation of these radiotracers is ongoing, several suffer from poor signal to background ratio or are not taken up by *S. aureus*[30], and none have so far progressed into clinical trials for the detection of *S. aureus* infection in humans.

One strategy to develop bacteria-specific radiotracers is to radiolabel compounds that are substrates for metabolic pathways that exist in bacteria but not in mammalian cells. Previously we reported the synthesis and PET imaging of 2-[^{18}F]F-PABA, an ^{18}F analog of *p*-amino benzoic acid (PABA).[12] PABA is the substrate for dihydropteroate synthase (DHPS), an enzyme in the bacterial folate biosynthesis pathway,[34] and we demonstrated that F-PABA is also a substrate for DHPS. We evaluated 2-[^{18}F]F-PABA in a rat model of *S. aureus* infection and found that the radiotracer accumulated in the infected triceps at an 8-

fold higher level than at the site of sterile inflammation in the contralateral triceps, but with low absolute uptake at the infected site (~ 0.2%ID/cc). More recently Mutch et al. reported the ^{11}C-labelling of PABA which gave an infected-to-inflamed tissue ratio of ~3 fold in a soft tissue infection model.[11] Both F-PABA and PABA were eliminated rapidly through the kidneys and were also susceptible to hepatic *N*-acetylation by the host. In an attempt to improve the pharmacokinetics of F-PABA and thus improve radiotracer uptake by *S. aureus*, we adopted a pro-drug approach in which the carboxylic acid group of F-PABA was protected by an ester and the amino group of F-PABA was replaced by the metabolically more stable nitro group. We hypothesized that ethyl 2-[^{18}F]F-4-nitro benzoate (2-[^{18}F]F-ENB) might be converted into 2-[^{18}F]F-PABA *in situ* through the reduction and hydrolysis of 2-[^{18}F]F-ENB by *S. aureus* nitroreductases and esterases, resulting in the metabolic trapping of the radiotracer through incorporation of the resulting 2-[^{18}F]F-PABA into folic acid by DHPS.

We analyzed the blood metabolites of 2-[^{18}F]F-ENB and found that the ethyl ester was rapidly and efficiently hydrolyzed to the 2-[^{18}F]F-NB acid in rat plasma both *in vitro* and in healthy rats whereas the aromatic nitro group was found to be more metabolically stable. We then evaluated both the ester 2-[^{18}F]F-ENB and the corresponding acid, 2-[^{18}F]F-NB, in a soft tissue model of *S. aureus* infection. PET imaging and *ex vivo* gamma counting demonstrated that both 2-[^{18}F]F-ENB and 2-[^{18}F]F-NB accumulated at the site of infection (*S. aureus* Newman) with a 17-fold difference in uptake between the infected triceps and the inflamed triceps (Figure 7), which is consistent with the observation of rapid hydrolysis of 2-[^{18}F]F-ENB to 2-[^{18}F]F-NB and supporting the proposal that the active tracer *in vivo* is 2-[^{18}F]F-NB. Subsequently, *in vivo* PET imaging results were confirmed by the colocalization of the *ex vivo* PET signal of two radiotracers with the bioluminescent signal arising from the bioluminescent Xen29 strain of *S. aureus*.

To evaluate the proposed mechanism of action, enzymatic assay showed both the ester and acid were found to be substrates for the *S. aureus* nitroreductase NfsB. In addition, we showed that both F-ENB and F-NB antagonize the antibacterial activity of the DHPS sulfonamide inhibitor sulfamethoxazole. Taken together, these observations support the proposal that 2-[^{18}F]F-ENB and 2-[^{18}F]F-NB are converted into 2-[^{18}F]F-PABA and accumulates at the site of infection through incorporation into folic acid.

The goal of protecting the 2-[^{18}F]F-PABA carboxylate with an ester was to decrease the polarity of the compound and reduce the rate of renal clearance thereby increasing the period for uptake of the tracer at the site of infection. Although we observed rapid hydrolysis of the 2-[^{18}F]F-ENB ethyl ester in rats, the ester was significantly more stable in human plasma ($t_{1/2}$ of 35 min compared to 2 min), suggesting that 2-[^{18}F]F-ENB may be a useful radiotracer for imaging infection in humans. Finally, while the nitro group of the second generation tracers was stable in both rat and human plasma, studies in non-human primates recapitulated the observation in healthy rats that the aromatic nitro group in 4-nitrobenzoic acid is preferentially metabolized by intestinal flora.[35] Further studies will be required to determine the relative stability of the F-ENB and F-NB nitro group in humans. One outstanding question is whether hypoxia caused by necrosis of the infected tissue may be partially responsible for the accumulation of the nitroaromatic radiotracers given the

paradigm that nitroimidazole-based radiotracers, for example ^{18}F-fluoromisonidazole (^{18}F-FMISO), are used to detect tumor hypoxia.[36] Future studies will examine this possibility.

The studies in rats showed that 2-[^{18}F]F-ENB and 2-[^{18}F]F-NB resulted in similar levels of radiotracer accumulation at the site of infection, consistent with the rapid hydrolysis of the ester group. To facilitate the clinical translation of 2-[^{18}F]F-ENB, we optimized the radiosynthesis of this tracer using a less sterically hindered precursor 2,4-dinitro benzonitrile with improved decay-corrected radiochemical yield. The entire radiosynthesis was automated using a GE Tracerlab FXN Pro Radiosynthesis Module which should facilitate the translation to the clinical applications.

CONCLUSION

Two second generation bacteria-specific PET tracers, 2-[^{18}F]F-ENB and 2-[^{18}F]F-NB, have been developed and evaluated as a diagnostic tool for identifying and localizing *S. aureus* which is a major cause of deep-seated infections. Mechanism of action studies support a mode of accumulation that involves the conversion of the tracers into 2-[^{18}F]F-PABA which is then incorporated into folic acid by the bacterial DHPS enzyme. The radiotracers are clinically promising since they can be easily radiosynthesized and demonstrate excellent (17-fold) contrast between the sites of infection and sterile inflammation. Although studies in a rat model of soft tissue infection gave similar levels of accumulation for both 2-[^{18}F]F-ENB and 2-[^{18}F]F-NB, the slower hydrolysis of the F-ENB ester in human compared to rat plasma suggests that protection of the carboxylate may alter the pharmacokinetics of the tracer in humans and modulate radiotracer accumulation in deep-seated infections.

METHODS

Study Design

The objective of this study was to synthesize and evaluate 2-[^{18}F]F-ENB and 2-[^{18}F]F-NB as noninvasive PET imaging diagnostic tools for identifying and localizing *S. aureus* infections *in vivo*. All protocols were approved by the Stony Brook Biosafety, Radiation Safety, and Animal Care and Use Committees, and all *in vivo* procedures were conducted under an IACUC approved protocol in compliance with the Animal Welfare Act and the Public Health Service Policy on Humane Care and Use of Laboratory Animals.

Bacterial Strains

Experiments utilized *S. aureus* Newman or a bioluminescent strain of *S. aureus* (Xen29, ATCC 12600) which contains a chromosomal copy of the modified *Photorhabdus luminescens* luxABCDE operon at a single integration site on the bacterial chromosome. *S. aureus* Xen29 was obtained from PerkinElmer.

Synthesis of ethyl 2-fluoro-4-nitrobenzoate (F-ENB)

Ethyl 2-fluoro-4-nitrobenzoate (F-ENB) was synthesized from 2-fluoro-4-nitrobenzoic acid (**1**) as shown in Scheme 1. 2-Fluoro-4-nitrobenzoic acid (200 mg, 0.943 mmol), EDC/HCl (199 mg, 1.037 mmol), DMAP (23 mg, 0.188 mmol), a drop of DMF were added to a 50 ml

RBF containing 15 ml DCM. The reaction mixture was stirred on ice for 30 min after which ethanol (2 mL) was added and the mixture stirred at room temperature overnight. After the reaction was shown to be complete by TLC (30% ethyl acetate in hexane), the crude product was purified by Combiflash using a silica gel column and petroleum ether and ethyl acetate (30% ethyl acetate in hexane) as the mobile phase to yield F-ENB. ^{1}H NMR (400 MHz, DMSO-d_6): δ 1.33 (t, J=7.09 Hz, 3 H), δ 4.37 (q, J=7.09 Hz, 2 H), δ 8.08 – 8.19 (m, 2 H), δ 8.23 (dd, J=10.51, 1.71 Hz, 1 H). ^{19}F NMR (376 MHz, DMSO-d_6): δ −106.99 (s, 1 F).

Synthesis of 2-fluoro-4-aminoacetophenone

2-Fluoro-4-aminoacetophenone (F-AAP) was synthesized from 2-fluoro-4-nitroacetophenone (**2**) as shown in Scheme 2. 2-Fluoro-4-nitroacetophenone (50 mg, 0.27 mmol), Zn powder (178 mg, 2.73 mmol), ammonium chloride (219 mg, 4.0 mmol) were added to a 50 ml RBF containing 4.5 ml methanol and 1 ml H_2O. The reaction mixture was heated at 85 °C for 30 min under reflux. After the reaction was shown to be complete by TLC (20% ethyl acetate in hexane), the reaction mixture was cooled to room temperature and the solvent was removed and the solid crude was resuspended in H_2O and extracted with ethyl acetate. The crude product was purified by Combiflash using a silica gel column and petroleum ether and ethyl acetate (20% ethyl acetate in hexane) as the mobile phase to yield F-AAP. ESI-MS calculated for molecular ion C_8H_9FNO ($[M + H]^+$): m/z = 154, found m/z = 154 in positive mode. ^{1}H NMR (400 MHz, $CDCl_3$-*d*): δ 2.56 (d, *J*=5.38 Hz, 3 H) 4.21 (br. s., 2 H) 6.31 (dd, *J*=13.20, 2.20 Hz, 1 H) 6.44 (dd, *J*=8.56, 2.20 Hz, 1 H) 7.77 (t, *J*=8.56 Hz, 1 H) (Figure S10).

Manual radiosynthesis of ethyl 2-[^{18}F]F-4-nitrobenzoate (2-[^{18}F]F-ENB)

The radiosynthesis of 2-[^{18}F]F-ENB was performed manually. Aqueous [^{18}F]fluoride in ddH_2O was trapped on a QMA cartridge and then eluted with a solution containing Kryptofix $K_{2.2.2}$ (7 mg) and potassium bicarbonate (2 mg) in 2 mL of acetonitrile (MeCN). The solvent was azeotropically evaporated under Argon, and 3 aliquots of MeCN (1 mL each) were successively added to the reaction vessel and then evaporated to afford a dry residue. The solid residue was re-solubilized with 0.5 mL DMSO containing precursor (5 mg). The reaction vessel was securely capped and the reaction mixture was stirred and heated at 95 °C for 10 min and subsequently diluted with H_2O and loaded onto a preconditioned Waters C18 Light SepPak cartridge. The crude reaction product was eluted from the SepPak cartridge with MeCN (0.5 mL) into a receiving vial preloaded with H_2O (0.5 mL). The resulting mixture was then loaded onto a semi-preparative HPLC column (Phenomenex Luna C18(2), 10 μm, 250 × 10 mm) and eluted with 45% MeCN/55% H_2O at a flow rate of 4 mL/min. The product fraction (eluting at 19–21 min) was collected and diluted with H_2O (30 mL). The diluted product solution was then passed through a second C18 Light SepPak cartridge. The final product was eluted from the SepPak with ethanol (0.3 mL) into a product vial pre-charged with USP saline (2.2 mL). Finally, the formulated product solution was passed through a membrane filter (Millipore Millex GV, 0.22 μm) into a vented sterile vial. A portion of the product solution was then taken to spike in the reference compound solution and analyzed with analytic HPLC (Phenomenex Luna C18(2), 10 μm, 250 × 4 mm, mobile phase: 45% MeCN/55% H_2O, flow rate: 0.8 mL/min) for quality control analysis.

Automated radiosynthesis of ethyl 2-[^{18}F]F-4-nitrobenzoate (2-[^{18}F]F-ENB)

[^{18}F]F-ENB was synthesized using a GE Tracerlab FXN pro radiosynthesis box. [^{18}F]Fluoride was produced at an offsite cyclotron and arrived at our facility around 4 h EOB. The [^{18}F] fluoride was trapped on a Waters Sep-Pak light Accell plus QMA cartridge and then eluted with 1 mL of 96% MeCN containing potassium carbonate (4 mg/mL) / Kryptofix $K_{2.2.2}$ (14.4 mg/mL) into the reaction vessel. This solution was evaporated to dryness under a stream of nitrogen at 70 °C for 7 min followed by 100 °C for 1 min. The reaction vial was cooled to 40 °C and 2.0 mg of 2,4- dinitrobenzonitrile in 1 mL DMSO was added. The reaction vessel was then sealed and stirred for 6 min after which the mixture was diluted with 8 mL of H_2O before being loaded onto conditioned Oasis HLB and Sep-Pak light C18 cartridges in series. The cartridges are then back flushed with 3 mL MeCN to elute the desired 2-[^{18}F]fluoro-4-nitrobenzonitrile which was returned to the original reaction vessel. The cartridges were eluted with 8 mL of H_2O so that they could be reused after the second reaction. The MeCN was removed under a stream of nitrogen gas at 60 °C for 5 min, and 1 mL of 2 M potassium hydroxide was added to the residue. The reaction vessel was then sealed and heated to 105 °C for 10 min, and then cooled to 40 °C before 2 mL of 2M acetic acid and 5 mL of H_2O were added. The mixture was stirred before being passed over previously used HLB and C18 cartridges. The cartridges were then back flushed with 1.5 ml MeCN to elute 2-[^{18}F]fluoro-4-nitrobenzoic acid to a second reaction vessel, and the MeCN was removed under a stream of nitrogen at 60 °C. Ethyl tosylate (50 μg) in 1.0 mL DMF/ saturated Na_2CO_3(aq) was then added to the second reaction vessel which was then sealed and heated to 105°C for 5 min. After cooling, 4.5 mL of H_2O was added to the reaction vessel, and the resulting mixture was then loaded onto a semi-preparative HPLC column (Phenomenex Luna C18(2), 10 μm, 250 × 10 mm) and eluted with 45% MeCN/55% H_2O at a flow rate of 5 mL/min. The product fraction was collected and diluted with H_2O (30 mL) and then passed through a second C18 Light SepPak cartridge. The final product was eluted from the SepPak with ethanol (1.0 mL) into a product vial pre-charged with USP saline (10 mL). Finally, the formulated product solution was passed through a membrane filter (Millipore Millex GV, 0.22 μm) into a vented sterile empty vial. A portion of the product solution was then taken for quality control tests as performed in the manual radiosynthesis procedure.

Automated radiosynthesis of 2-[^{18}F]F-4-nitrobenzoate (2-[^{18}F]F-NB)

2-[^{18}F]F-NB was synthesized using a GE Tracerlab FXN pro radiosynthesis box. [^{18}F]Fluoride was produced at an offsite cyclotron and arrived at our facility around 4 h EOB. The [^{18}F] fluoride was trapped on a Waters Sep-Pak light Accell plus QMA cartridge and then eluted with 1 mL of 96% MeCN containing potassium carbonate (4 mg/mL) / Kryptofix $K_{2.2.2}$ (14.4 mg/mL) into the reaction vessel. This solution was evaporated to dryness under a stream of nitrogen at 70 °C for 7 min followed by 100 °C for 1 min. The reaction vial was cooled to 40 °C and 2.0 mg of 2,4- dinitrobenzonitrile in 1 mL DMSO was added. The reaction vessel was sealed and stirred for 6 min after which the mixture was diluted with 8 mL of H_2O before being loaded onto conditioned Oasis HLB and Sep-Pak light C18 cartridges in series. The cartridges were then back flushed with 3 mL MeCN to elute the desired 2-[^{18}F]fluoro-4-nitrobenzonitrile which was returned to the original reaction vessel. The cartridges were then eluted with 8 mL of H_2O so that they could be

reused after the second reaction. The MeCN was removed under a stream of nitrogen gas at 60 °C for 5 min, and 1 mL of 2 M potassium hydroxide was added to the residue. The reaction vessel was sealed and heated to 105 °C for 10 min after which it was then cooled to 40 °C before 2 mL of 2M acetic acid and 2 mL of H_2O were added. The mixture was loaded onto a semi-preparative HPLC column (Phenomenex Luna C18(2), 10 μm, 250 × 10 mm) and eluted with 25% MeCN containing 0.1% TFA at a flow rate of 5 mL/min. The product fraction (eluting at 14–16 min) was collected and diluted with H_2O (30 mL). The diluted product solution was passed through a second HLB SepPak cartridge. The final product, 2-[^{18}F] fluoro-4-nitrobenzoic acid, was eluted from the SepPak with ethanol (1.0 mL) into a product vial pre-charged with USP saline (10 mL). Finally, the formulated product solution was passed through a membrane filter (Millipore Millex GV, 0.22 μm) into a vented sterile empty vial. A portion of the product solution was then taken for quality control tests as described in the manual radiosynthesis procedure.

The nitroreductase assay

NfsB was expressed and purified as described previously.[24] The nitroreductase assay was performed at room temperature in 50 mM Tris-HCl buffer, pH 7.4, containing 5 mM EDTA in a total reaction volume of 500 μL. Reactions were initiated by the addition of NfsB to a final concentration of 45 nM, and the consumption of NADH was continuously monitored at 340 nm. The k_{cat} and K_m values were determined at a fixed concentration of NADH (60 μM NADH for NfsB) by varying the concentration of 2-F-ENB, 2-F-NB or 2-F-NAP. The experiments were performed in triplicate and the initial velocities as a function of substrate concentration were globally fit to the Michaelis–Menten equation using GraphPad Prism 4.

In vitro cellular uptake of radiotracer

S. aureus Newman and *S. aureus* Xen 29 were aerobically grown to OD600 0.6 in LB media at 37 °C. To evaluate the uptake of 2-[^{18}F]F-NB, the bacteria were incubated with 1 μCi/mL of the radiotracer at 37°C with rapid agitation. Heat-killed (90°C for 30 min) bacteria were similarly incubated with 2-[^{18}F]F-NB. Aliquots (1 mL) were removed after 5 min, 30 min, 60 min, 90 min, and 120 min and pelleted by centrifugation (11000 RPM, 3 min) and washed three times with cold phosphate buffered saline (PBS). Total radioactivity was measured using an automated gamma counter and is reported as the percentage of radioactivity added to the culture. A minimum of five replicates were used for each assay and time point.

Minimum Inhibitory Concentration (MIC)

Antibacterial susceptibility tests for aerobically growing bacteria were performed with the microbroth dilution assay according to the Clinical and Laboratory Standard Institute in transparent 96-well plates[37]. *S. aureus* Xen 29 (PerkinElmer) were utilized in this study. Briefly, bacteria were grown to mid-log phase (OD600 of 0.6–0.7) in cation-adjusted Mueller-Hinton (CAMH) media at 37 °C in an orbital shaker. Subsequently, bacteria were re-suspended in the M9 media. A final concentration of 10^6 CFU/mL per well was added to M9 media (1% glucose, 1% casaminoacids, 1mM thiamine, 0.05 mM nicotinamide, 2mM $MgCl_2$, 0.1 mM $CaCl_2$) containing 2-fold dilutions of SMX to give final concentrations ranging from 0.05 to 100 μg/mL either alone or in the presence of PABA (0.8 μg/mL and 4

μg/mL), F-PABA (0.8 μg/mL and 4 μg/mL), F-NB (10 μg/mL, 20 μg/mL and 40 μg/mL), or F-NAP (10 μg/mL, 20 μg/mL and 40 μg/mL). The plate was examined for bacteria growth using a UV-vis plate reader after 24 h incubation at 37 °C. The MIC was recorded as the lowest SMX concentration (μM) required to inhibit at least 90% of bacterial growth as judged by the absorbance of the culture media.

In vitro metabolic stability of the radiotracers in rat plasma

2-[^{18}F]F-ENB (600 μCi) was incubated with Sprague Dawley rat plasma (5.0 mL) at 37 °C. Subsequently, 0.4 mL aliquots of the plasma were taken 2, 10, 30, and 85 min after addition of the tracer, and 0.6 mL of MeCN was added to quench the metabolism. The mixture was centrifuged at 13,400 rpm for 10 min to remove proteins, and both the supernatant and the protein pellet were analyzed by gamma counting to calculate the extraction efficiency. The supernatant was spiked with 50 μL cold standards (F-PABA, 2-fluoro-4-nitrobenzoic acid, ethyl 2-fluoro-4-aminobenzoate, ethyl 2-fluoro-4-nitrobenzoate, 1 mg/ml) and injected onto a semi-prep HPLC column (Phenomenex Luna C18(2), 10 μm, 250 × 10 mm) that was then eluted with 45% MeCN/55% H_2O, 0.1% trifluoroacetic acid, at a flow rate of 4 mL/min. The radioactive fractions corresponding to each cold standard were collected and radioactivity was quantified using a gamma counter from which the percentage of each metabolite was calculated.

In vitro metabolic stability of the radiotracers in human plasma

2-[^{18}F]F-ENB (600 μCi) was incubated with 5.0 mL human serum (catalog #: H4522 from Sigma) at 37 °C. Subsequently, 0.4 mL aliquots of the plasma were taken 2, 10, 30, and 85 min after addition of the tracer, and 0.6 mL of MeCN was added to quench the metabolism. The mixture was centrifuged at 13,400 rpm for 10 min to remove proteins, and both the supernatant and the protein pellet were analyzed by gamma counting to calculate the extraction efficiency. The supernatant was spiked with 50 μL cold standards (F-PABA, 2-fluoro-4-nitrobenzoic acid, ethyl 2-fluoro-4-aminobenzoate, ethyl 2-fluoro-4-nitrobenzoate, 1 mg/ml) and injected onto a semi-prep HPLC column (Phenomenex Luna C18(2), 10 μm, 250 × 10 mm) that was then eluted with 45% MeCN/55% H_2O, 0.1% trifluoroacetic acid, at a flow rate of 4 mL/min. The radioactive fractions corresponding to each cold standard were collected and the radioactivity was counted using a gamma counter from which the percentage of each metabolite was calculated (n=3).

In vivo metabolite analysis

2-[^{18}F]F-ENB (1 mCi) was injected via the tail vein into healthy female Sprague–Dawley rats (10 weeks old, Charles River). At 5, 30, and 60 min (n=3 rats at each time point), 1 mL of blood was obtained by cardiac puncture, centrifuged, and 50 μL of each standard (including N-acetyl F-PABA, F-PABA, 2-fluoro-4-nitrobenzoic acid, ethyl 2-fluoro-4-aminobenzoate and ethyl 2-fluoro-4-nitrobenzoate, 1 mg/mL) was added to 0.4 mL aliquots of the resulting supernatant together with 0.6 mL MeCN. The mixture was centrifuged at 13,400 rpm for 5 min to remove the protein, and the supernatant and protein pellet were analyzed by gamma counter to determine the efficiency of extraction. The supernatant was injected onto a semi-prep HPLC column (Phenomenex Luna C18(2), 10 μm, 250 × 10 mm) and chromatography was performed with 45% MeCN/55% H_2O containing 0.1%

trifluoroacetic acid, at a flow rate of 4 mL/min. The radioactive fractions corresponding to each cold standard were collected and analyzed using a gamma counter from which the percentage of each metabolite was calculated (n=3).

Analysis of the radioactive metabolites in the urine was performed using a similar procedure from samples obtained from the bladder 30 and 60 min after tracer injection. The urine was diluted with 45% MeCN/H_2O, centrifuged at 13400 rpm for 5 min and spiked with cold standards for radio-HPLC analysis.

Rat triceps infection

S. aureus (Newman or Xen29) was cultured overnight by inoculating 5 μL of bacteria from a glycerol stock into 10 mL of fresh Cation-Adjusted Mueller Hinton (CAMH) broth or tryptic soy broth (TSB). One hundred μL of the overnight culture was then used to inoculate 5 mL of fresh CAMH media or TSB media which was shaken at 37 °C for about 2 h until the culture reached an OD of 0.6. A 0.5 mL sample of the culture was subsequently centrifuged at 11,000 RPM for 3 min and the cell pellet was washed twice with 0.5 mL brain heart infusion (BHI) media before being resuspended in 0.15 mL BHI media. Healthy female Sprague–Dawley rats (10 weeks old, Charles River) were intramuscularly infected with *S. aureus* Newman or Xen29 in the right triceps with a bacterial burden of 8 $\log_{10}$ CFU (50 μL BHI culture). The rats were imaged by PET/CT 22 to 24 h after infection. After imaging, the infected triceps were collected, homogenized in PBS using a hand-held homogenizer, and the bacterial burden at the time of imaging was determined by plating the muscle tissues onto solid MH medium. After overnight incubation at 37 °C, CFUs were quantified by enumeration. For histological examination, tissue samples were also obtained from some of the infected animals, fixed overnight in 4% formaldehyde before being embedded in paraffin, sectioned at 4 μm, and stained with hematoxylin and eosin (H&E) or Gram stain.

Sterile inflammation in the rat triceps

S. aureus (Newman or Xen29) was cultured as described above except that an additional culture was autoclaved to generate a sample of heat-killed bacteria. One mL of the autoclaved culture was centrifuged at 11,000 rpm for 3 min, and the cell pellet was washed twice with 1 mL BHI and then resuspended in 0.15 mL BHI. Female Sprague–Dawley rats were injected with 50 μL of the heat killed bacterial culture to induce inflammation in the left triceps. To confirm the absence of live bacterial cells present in the left triceps, the triceps were collected after imaging, homogenized and plated for CFU counting. A histological examination was also conducted as described above after imaging to confirm the presence of inflammation.

PET/CT Imaging

2-[^{18}F]F-ENB or 2-[^{18}F]F-NB(600 to 1000 μCi) was injected via a tail vein catheter into rats that were anesthetized using 2% isoflurane with oxygen. Immediately after tracer administration, a 120 min dynamic PET scan was performed, followed by an 8 min full-body CT scan using a SIEMENS Inveon™ Docked PET/SPECT/CT. The CT data were reconstructed in real-time in voxel numbers that was automatically calculated by the software. After the imaging, the PET data were histogrammed into designated time frames,

followed by reconstruction into PET images using the OSEM 3D method. The images were subsequently analyzed by Amide version 1.0.4 (http://www.amide.sourceforge.net).

After the 120-min dynamic scan was complete, the rats were returned to their cages for 1 h to allow them to recover from anesthesia. Three h after tracer injection, a 20 min static PET scan was performed followed by an 8 min full-body CT scan. The image data were reconstructed and analyzed in the same way as 120 min dynamic scan.

After completion of the whole-body scan, the rats were euthanized by CO_2 inhalation and the infected and inflamed triceps were excised and subsequently imaged with PET/CT scanner for 20 min. The image data were analyzed with Amide. The rest of the major organs were dissected and collected for *ex vivo* gamma counting described below.

For [^{18}F]FDG PET imaging, rats were fasted 12 h before they were injected with 800 μCi of radiotracer via the tail vein. The animals were allowed to wake up between [^{18}F]FDG injection and imaging, and PET scanning was performed 1 h after tracer administration using a 20-min list mode acquisition. The image data were reconstructed and analyzed in the same way as described above.

Bioluminescence imaging

Upon completion of PET/CT imaging of excised infected and inflamed triceps, the same triceps were imaged with the IVIS Lumina II imaging station. Image data collection was performed using a field of view of 8 or 10 cm, exposure time of 5 min, binning number of 16, and an f1/stop of 1. The image analysis was performed with the Living Image software package. The signal intensity of the region of interest (ROI) is represented by radiance (p/sec/cm2/sr), which refers to the number of photons per second that are leaving a square centimeter of tissue and radiating into a solid angle of one steradian (sr).

Ex vivo radiotracer biodistribution

The biodistribution study was performed after the completion of *ex vivo* tissue PET/CT imaging and bioluminescence imaging described above. The major organs and tissues were collected, weighed and placed in gamma counter tubes. The organ-associated radioactivity was measured using a gamma counter (Wizard 2480, PerkinElmer) and is expressed as %ID/g (percentage of injected dose per gram of organ).

Supplementary Material

Refer to Web version on PubMed Central for supplementary material.

ACKNOWLEDGMENTS

This work was supported by NIH grants EB024549 and EB027050 to P.J.T.

REFERENCES

(1). Tong SY, Davis JS, Eichenberger E, Holland TL and Fowler VG Jr. (2015) Staphylococcus aureus infections: epidemiology, pathophysiology, clinical manifestations, and management. Clin Microbiol Rev. 28, 603–661. [PubMed: 26016486]

(2). Signore A and Glaudemans AW (2011) The molecular imaging approach to image infections and inflammation by nuclear medicine techniques. Ann Nucl Med. 25, 681–700. [PubMed: 21837469]

(3). Censullo A and Vijayan T (2017) Using Nuclear Medicine Imaging Wisely in Diagnosing Infectious Diseases. Open Forum Infect Dis. 4, ofx011. [PubMed: 28480283]

(4). Jamar F, Buscombe J, Chiti A, Christian PE, Delbeke D, Donohoe KJ, Israel O, Martin-Comin J and Signore A (2013) EANM/SNMMI guideline for 18F-FDG use in inflammation and infection. J Nucl Med. 54, 647–658. [PubMed: 23359660]

(5). Meller J, Sahlmann CO and Scheel AK (2007) 18F-FDG PET and PET/CT in fever of unknown origin. J Nucl Med. 48, 35–45. [PubMed: 17204697]

(6). Palestro CJ, Love C and Bhargava KK (2009) Labeled leukocyte imaging: current status and future directions. Q J Nucl Med Mol Imaging. 53, 105–123. [PubMed: 19182734]

(7). Ordonez AA and Jain SK (2018) Pathogen-Specific Bacterial Imaging in Nuclear Medicine. Semin Nucl Med. 48, 182–194. [PubMed: 29452620]

(8). Auletta S, Varani M, Horvat R, Galli F, Signore A and Hess S (2019) PET Radiopharmaceuticals for Specific Bacteria Imaging: A Systematic Review. J Clin Med. 8.

(9). Northrup JD, Mach RH and Sellmyer MA (2019) Radiochemical Approaches to Imaging Bacterial Infections: Intracellular versus Extracellular Targets. Int J Mol Sci. 20.

(10). Sellmyer MA, Lee I, Hou C, Weng CC, Li S, Lieberman BP, Zeng C, Mankoff DA and Mach RH (2017) Bacterial infection imaging with [(18)F]fluoropropyl-trimethoprim. Proc Natl Acad Sci U S A. 114, 8372–8377. [PubMed: 28716936]

(11). Mutch CA, Ordonez AA, Qin H, Parker M, Bambarger LE, Villanueva-Meyer JE, Blecha J, Carroll V, Taglang C, Flavell R, Sriram R, VanBrocklin H, Rosenberg O, Ohliger MA, Jain SK, Neumann KD and Wilson DM (2018) [(11)C]Para-Aminobenzoic Acid: A Positron Emission Tomography Tracer Targeting Bacteria-Specific Metabolism. ACS Infect Dis. 4, 1067–1072. [PubMed: 29712422]

(12). Zhang Z, Ordonez AA, Wang H, Li Y, Gogarty KR, Weinstein EA, Daryaee F, Merino J, Yoon GE, Kalinda AS, Mease RC, Iuliano JN, Smith-Jones PM, Jain SK and Tonge PJ (2018) Positron Emission Tomography Imaging with 2-[(18)F]F-p-Aminobenzoic Acid Detects Staphylococcus aureus Infections and Monitors Drug Response. ACS Infect Dis. 4, 1635–1644. [PubMed: 30067329]

(13). Zachariah PK and Juchau MR (1974) The role of gut flora in the reduction of aromatic nitro-groups. Drug Metab Dispos. 2, 74–78. [PubMed: 4150138]

(14). Wheeler LA, Soderberg FB and Goldman P (1975) The relationship between nitro group reduction and the intestinal microflora. J Pharmacol Exp Ther. 194, 135–144. [PubMed: 1097637]

(15). Wong RH, Kwong T, Yau KH and Au-Yeung HY (2015) Real time detection of live microbes using a highly sensitive bioluminescent nitroreductase probe. Chem Commun (Camb). 51, 4440–4442. [PubMed: 25680085]

(16). Xu S, Wang Q, Zhang Q, Zhang L, Zuo L, Jiang JD and Hu HY (2017) Real time detection of ESKAPE pathogens by a nitroreductase-triggered fluorescence turn-on probe. Chem Commun (Camb). 53, 11177–11180. [PubMed: 28953270]

(17). Vorobyeva AG, Stanton M, Godinat A, Lund KB, Karateev GG, Francis KP, Allen E, Gelovani JG, McCormack E, Tangney M and Dubikovskaya EA (2015) Development of a Bioluminescent Nitroreductase Probe for Preclinical Imaging. PLoS One. 10, e0131037. [PubMed: 26110789]

(18). Stanton M, Cronin M, Lehouritis P and Tangney M (2015) In vivo bacterial imaging without engineering; A novel probe-based strategy facilitated by endogenous nitroreductase enzymes. Curr Gene Ther. 15, 277–288. [PubMed: 25619884]

(19). Liu Y, Zhang L, Nazare M, Yao Q and Hu HY (2018) A novel nitroreductase-enhanced MRI contrast agent and its potential application in bacterial imaging. Acta Pharm Sin B. 8, 401–408. [PubMed: 29881679]

(20). Antunes IF, Haisma HJ, Elsinga PH, Sijbesma JW, Waarde A, Willemsen AT, Dierckx RA and de Vries EF (2012) In vivo evaluation of [18F]FEAnGA-Me: a PET tracer for imaging beta-

glucuronidase (beta-GUS) activity in a tumor/inflammation rodent model. Nucl Med Biol. 39, 854–863. [PubMed: 22445742]

(21). Xiong YQ, Willard J, Kadurugamuwa JL, Yu J, Francis KP and Bayer AS (2005) Real-time in vivo bioluminescent imaging for evaluating the efficacy of antibiotics in a rat Staphylococcus aureus endocarditis model. Antimicrob Agents Chemother. 49, 380–387. [PubMed: 15616318]

(22). Hertlein T, Sturm V, Lorenz U, Sumathy K, Jakob P and Ohlsen K (2014) Bioluminescence and 19F magnetic resonance imaging visualize the efficacy of lysostaphin alone and in combination with oxacillin against Staphylococcus aureus in murine thigh and catheter-associated infection models. Antimicrob Agents Chemother. 58, 1630–1638. [PubMed: 24366730]

(23). van Oosten M, Schafer T, Gazendam JA, Ohlsen K, Tsompanidou E, de Goffau MC, Harmsen HJ, Crane LM, Lim E, Francis KP, Cheung L, Olive M, Ntziachristos V, van Dijl JM and van Dam GM (2013) Real-time in vivo imaging of invasive- and biomaterial-associated bacterial infections using fluorescently labelled vancomycin. Nat Commun. 4, 2584. [PubMed: 24129412]

(24). Si Y, Basak S, Li Y, Merino J, Iuliano JN, Walker SG and Tonge PJ (2019) Antibacterial Activity and Mode of Action of a Sulfonamide-Based Class of Oxaborole Leucyl-tRNA-Synthetase Inhibitors. ACS Infect Dis. 5, 1231–1238. [PubMed: 31007018]

(25). Zenno S, Koike H, Kumar AN, Jayaraman R, Tanokura M and Saigo K (1996) Biochemical characterization of NfsA, the Escherichia coli major nitroreductase exhibiting a high amino acid sequence homology to Frp, a Vibrio harveyi flavin oxidoreductase. J Bacteriol. 178, 4508–4514. [PubMed: 8755878]

(26). Panizzi P, Nahrendorf M, Figueiredo JL, Panizzi J, Marinelli B, Iwamoto Y, Keliher E, Maddur AA, Waterman P, Kroh HK, Leuschner F, Aikawa E, Swirski FK, Pittet MJ, Hackeng TM, Fuentes-Prior P, Schneewind O, Bock PE and Weissleder R (2011) In vivo detection of Staphylococcus aureus endocarditis by targeting pathogen-specific prothrombin activation. Nat Med. 17, 1142–1146. [PubMed: 21857652]

(27). Hernandez FJ, Huang L, Olson ME, Powers KM, Hernandez LI, Meyerholz DK, Thedens DR, Behlke MA, Horswill AR and McNamara JO 2nd. (2014) Noninvasive imaging of Staphylococcus aureus infections with a nuclease-activated probe. Nat Med. 20, 301–306. [PubMed: 24487433]

(28). Ning X, Seo W, Lee S, Takemiya K, Rafi M, Feng X, Weiss D, Wang X, Williams L, Camp VM, Eugene M, Taylor WR, Goodman M and Murthy N (2014) PET imaging of bacterial infections with fluorine-18-labeled maltohexaose. Angew Chem Int Ed Engl. 53, 14096–14101. [PubMed: 25330976]

(29). Gowrishankar G, Namavari M, Jouannot EB, Hoehne A, Reeves R, Hardy J and Gambhir SS (2014) Investigation of 6-[(1)(8)F]-fluoromaltose as a novel PET tracer for imaging bacterial infection. PLoS One. 9, e107951. [PubMed: 25243851]

(30). Weinstein EA, Ordonez AA, DeMarco VP, Murawski AM, Pokkali S, MacDonald EM, Klunk M, Mease RC, Pomper MG and Jain SK (2014) Imaging Enterobacteriaceae infection in vivo with 18F-fluorodeoxysorbitol positron emission tomography. Sci Transl Med. 6, 259ra146.

(31). Gowrishankar G, Hardy J, Wardak M, Namavari M, Reeves RE, Neofytou E, Srinivasan A, Wu JC, Contag CH and Gambhir SS (2017) Specific Imaging of Bacterial Infection Using 6”-(18)F-Fluoromaltotriose: A Second-Generation PET Tracer Targeting the Maltodextrin Transporter in Bacteria. J Nucl Med. 58, 1679–1684. [PubMed: 28490473]

(32). Neumann KD, Villanueva-Meyer JE, Mutch CA, Flavell RR, Blecha JE, Kwak T, Sriram R, VanBrocklin HF, Rosenberg OS, Ohliger MA and Wilson DM (2017) Imaging Active Infection in vivo Using D-Amino Acid Derived PET Radiotracers. Sci Rep. 7, 7903. [PubMed: 28801560]

(33). Parker MFL, Luu JM, Schulte B, Huynh TL, Stewart MN, Sriram R, Yu MA, Jivan S, Turnbaugh PJ, Flavell RR, Rosenberg OS, Ohliger MA and Wilson DM (2020) Sensing Living Bacteria in Vivo Using d-Alanine-Derived (11)C Radiotracers. ACS Cent Sci. 6, 155–165. [PubMed: 32123733]

(34). Wegkamp A, van Oorschot W, de Vos WM and Smid EJ (2007) Characterization of the role of para-aminobenzoic acid biosynthesis in folate production by Lactococcus lactis. Appl Environ Microbiol. 73, 2673–2681. [PubMed: 17308179]

(35). Kuzniar EJ and James SP (1981) Influence of the gut microflora on the metabolism of 4-nitrobenzoic acid in the marmoset. Xenobiotica. 11, 675–683. [PubMed: 6976659]

(36). Lopci E, Grassi I, Chiti A, Nanni C, Cicoria G, Toschi L, Fonti C, Lodi F, Mattioli S and Fanti S (2014) PET radiopharmaceuticals for imaging of tumor hypoxia: a review of the evidence. Am J Nucl Med Mol Imaging. 4, 365–384. [PubMed: 24982822]

(37). CLSI. (2006) Approved Standard M7-A5, 6 ed., Clinical and Laboratory Standards Institute, Wayne, PA.

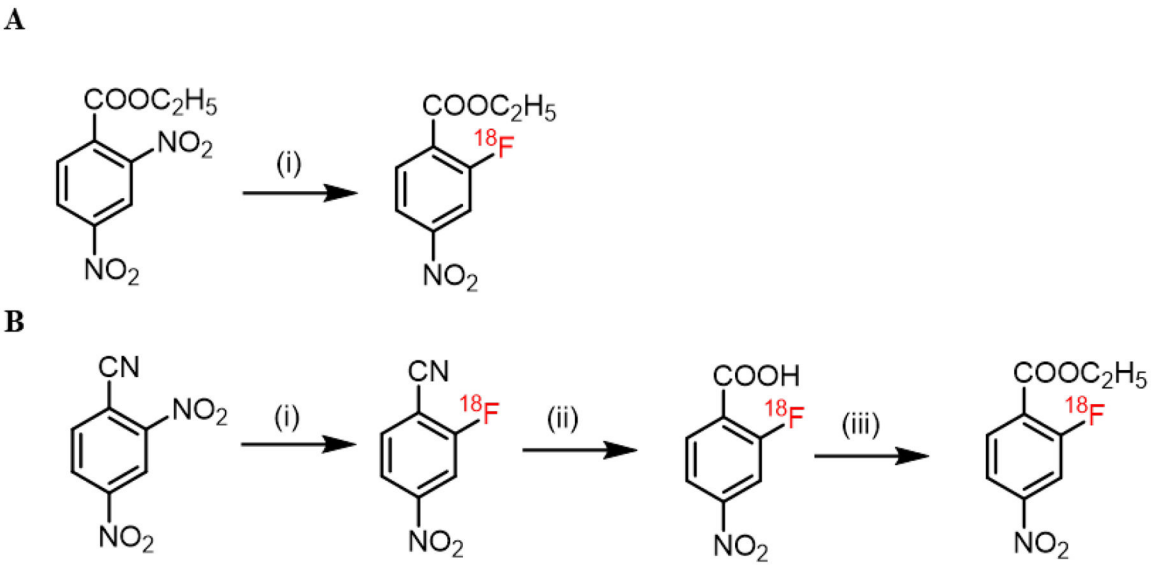

Figure 1: Radiosynthesis of 2-[^{18}F]F-ENB.

(A) Manual synthesis: (i): [^{18}F]potassium fluoride, Kryptofix$_{222}$, potassium carbonate, dimethyl sulfoxide, 95 °C, 10 min. (B) Automated synthesis: (i):[^{18}F]potassium fluoride, Kryptofix$_{222}$, potassium carbonate, dimethyl sulfoxide, r.t., 10 min; (ii): 2M potassium hydroxide in H_2O, 105 °C, 10 min; (iii): ethyl tosylate, potassium carbonate, dimethylformamide, 110 °C, 10 min.

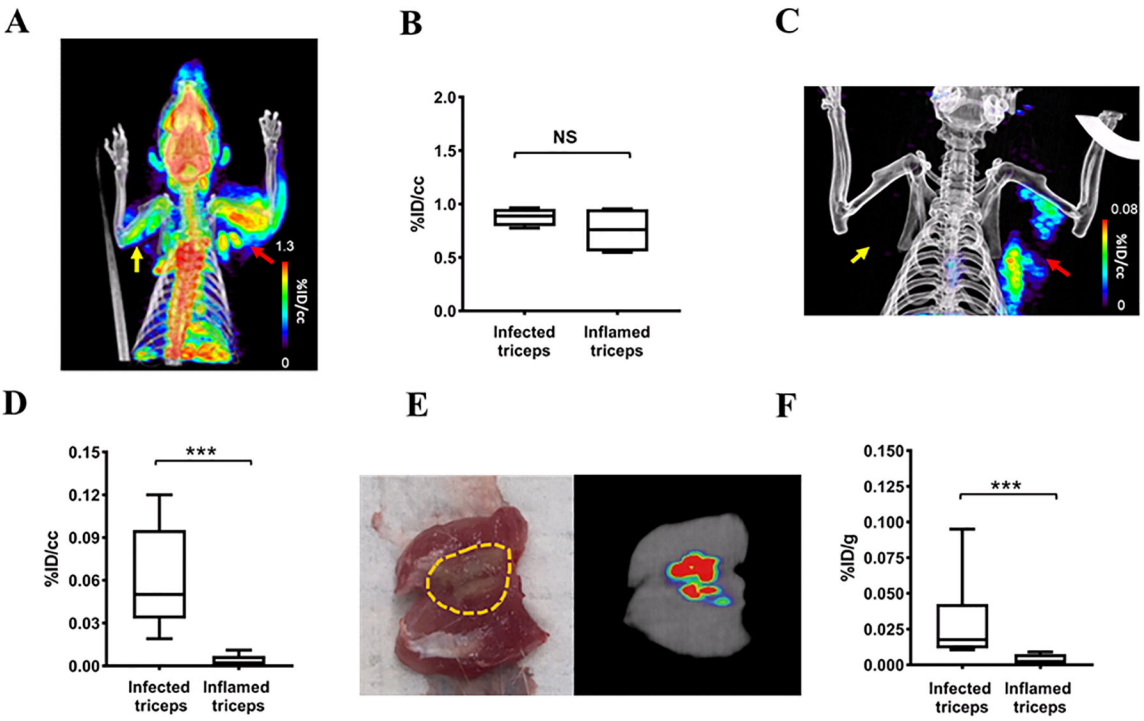

Figure 2: PET/CT imaging of a rat model of *S. aureus Newman*-induced triceps infection.

(A) [^{18}F]FDG PET/CT of a rat in which 8.2 ± 0.2 log10 CFU of *S. aureus Newman* has been injected into the right triceps (red arrow) and with sterile inflammation in the left triceps (yellow arrow). The image was acquired 60–80 min after tracer injection. (B) Comparison of [^{18}F]FDG accumulation 60–80 min post-injection at sites of infection and sterile inflammation, represented as % injected dose per cc (%ID/cc). (C) 2-[^{18}F]F-ENB accumulation was observed in the infected (red arrow) but not inflamed triceps (yellow arrow) 180–200 min after tracer injection. (D) Comparison of 2-[^{18}F]F-ENB accumulation in the infected triceps and inflamed triceps 180–200 min after tracer injection: ***P < 0.001 from a two-tailed Mann-Whitney U Test (n = 7). (E) *Ex vivo* PET imaging of the excised infected triceps. The area of infection is highlighted in yellow. (F) Post-mortem *ex vivo* analysis of 2-[^{18}F]F-ENB biodistribution at sites of infection and sterile inflammation 3 h after tracer injection, represented as % injected dose per gram (%ID/g): ***P < 0.001 from a two-tailed Mann-Whitney U Test (n = 8).

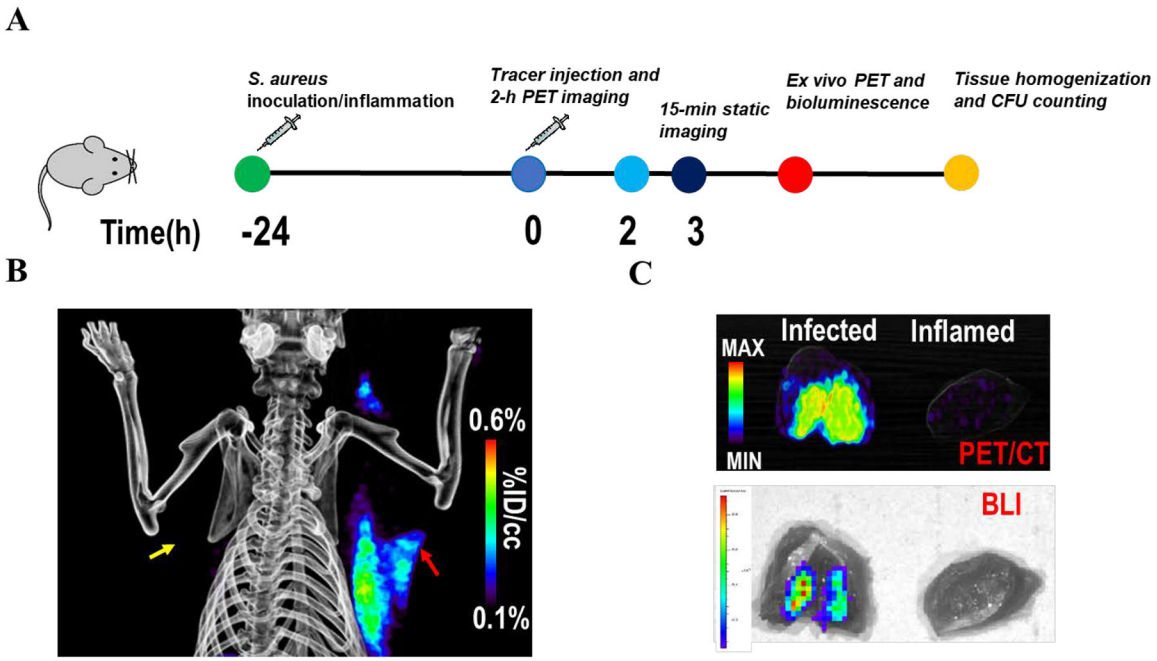

Figure 3: PET/CT imaging of rats infected in the right triceps with the bioluminescent Xen29 strain of *S. aureus*.

(A) Experimental design. (B) 2-[^{18}F]F-ENB-derived radioactivity accumulates in the infected triceps (red arrow) but not the inflamed triceps (yellow arrow) at 3 h post tracer administration. (C) *Ex vivo* PET/CT imaging and bioluminescent imaging of the excised triceps demonstrated that the radioactivity in the infected triceps co-localized with the bioluminescence signal generated by *S. aureus* Xen29.

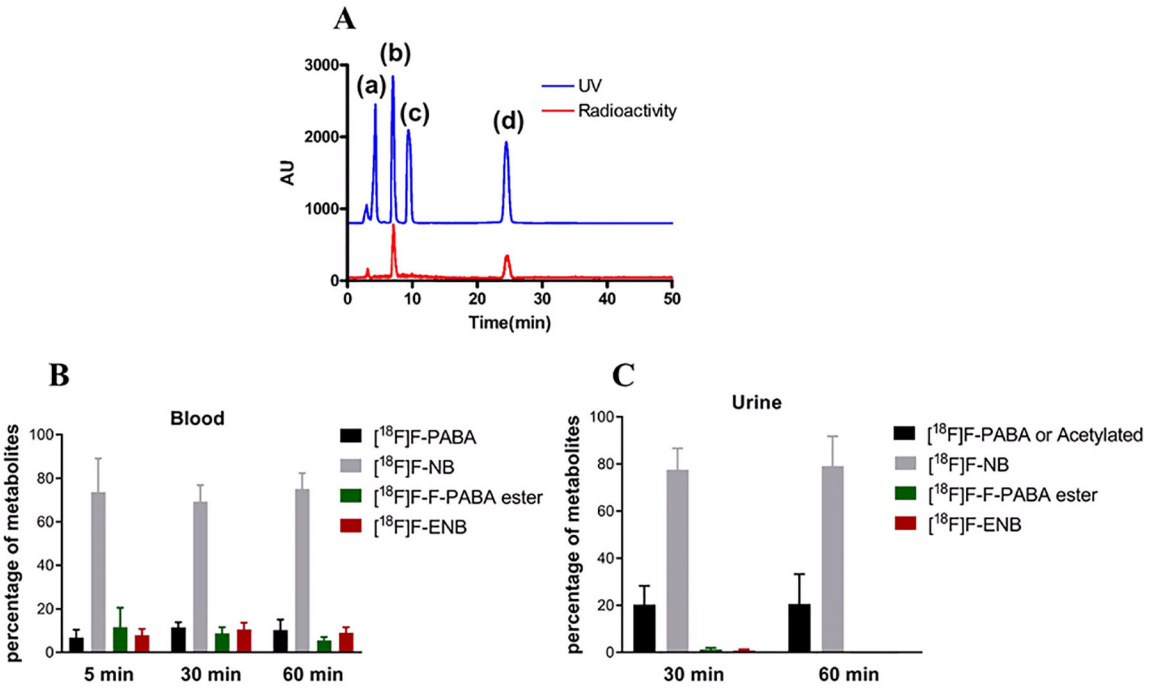

Figure 4: Analysis of metabolites in the plasma and urine of healthy rats after intravenous injection (IV) of 2-[^{18}F]F-ENB.

After IV administration of 2-[^{18}F]F-ENB, the animals were sacrificed at each time point (n = 3 rats) and the blood and urine samples were collected for radio-HPLC analysis. (A) A representative HPLC chromatogram is shown to illustrate the separation of four major non-radioactive cold standards: 2-F-PABA (a), 2-F-NB (b), 2-F-PABA ester (c) and 2-F-ENB (d). The red trace is the HPLC chromatogram of a blood sample that reveals the presence of 2-[^{18}F]F-NB and 2-[^{18}F]F-ENB. The percent of each metabolite in blood (B) and urine (C) is shown.

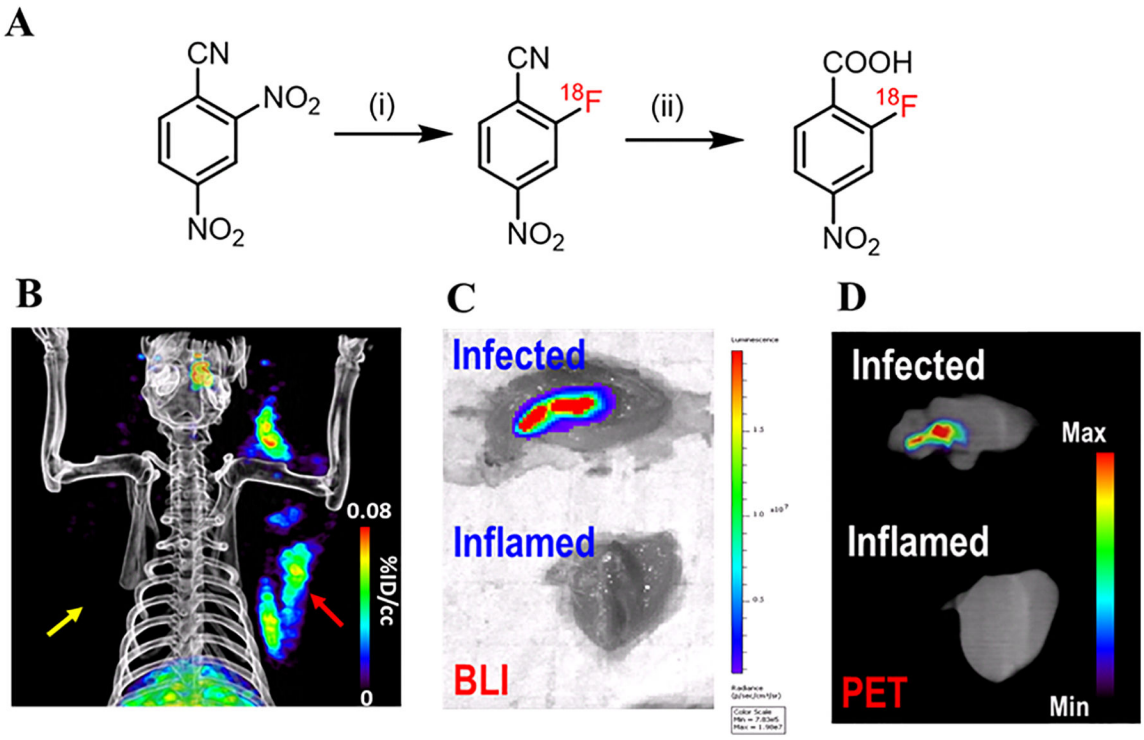

Figure 5: PET/CT imaging of 2-[^{18}F]F-NB in a rat model of *S. aureus* Xen29 infection.

(A) Radiosynthesis of 2-[^{18}F]F-NB. (i): [^{18}F]potassium fluoride, Kryptofix$_{222}$, potassium carbonate, dimethyl sulfoxide, r.t., 10 min; (ii): 2M potassium hydroxide in H_2O, 105 °C, 10 min; Overall decay-corrected radiochemical yield: 26% (n = 1). (B) Accumulation of 2-[^{18}F]F-NB-derived radioactivity was observed in the infected (red arrow) but not inflamed triceps (yellow arrow). (C) *Ex vivo* bioluminescence and (D) PET/CT imaging of excised triceps showed that the radioactivity in the infected triceps colocalized with the bioluminescent signal emitted by the *S. aureus* Xen29 strain.

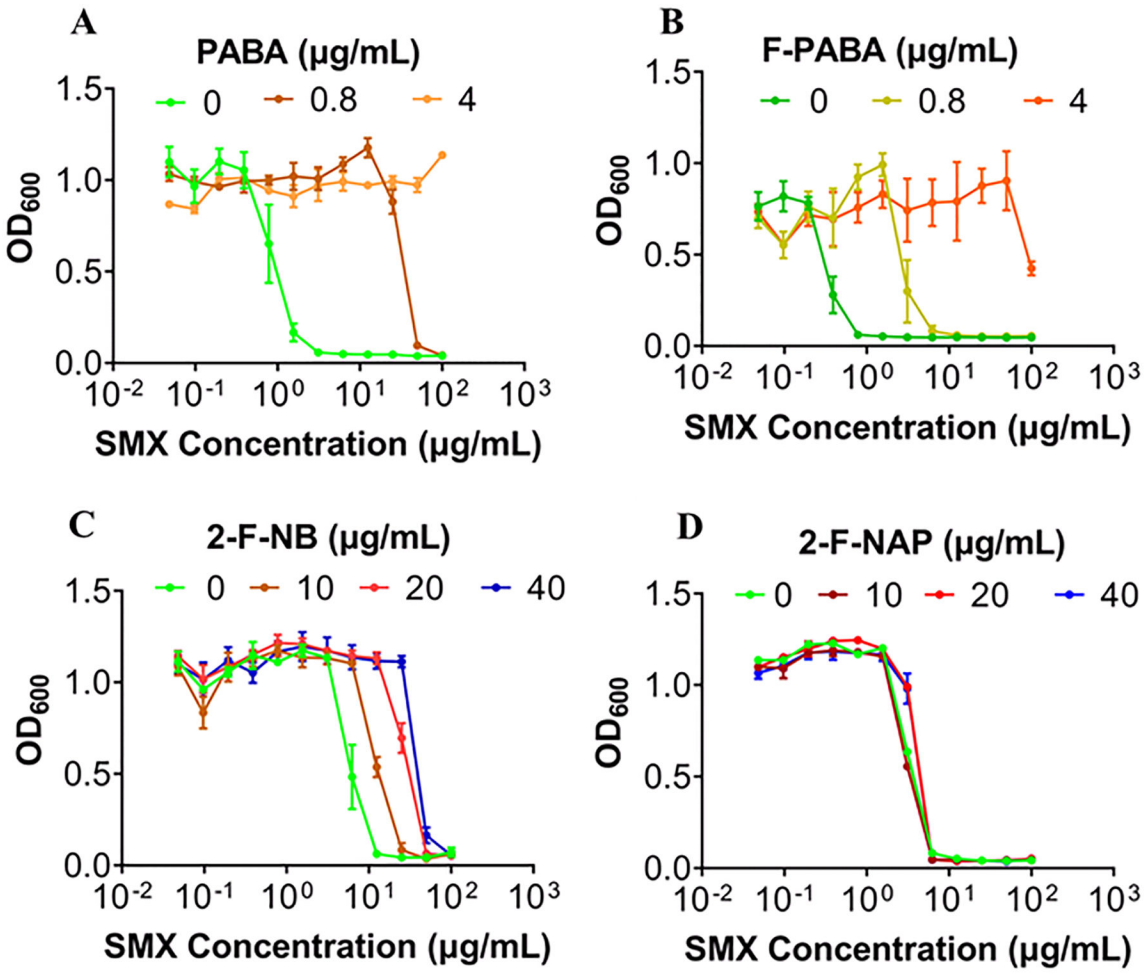

Figure 6: Impact of PABA analogs on the antibacterial activity of sulfamethoxazole (SMX)

(A) *S. aureus* Xen29 were incubated with SMX (0.048 μg/mL −100 μg/mL) either alone or in the presence of PABA (0.8 μg/mL and 4 μg/mL) demonstrating that PABA can rescue the inhibition of growth caused by SMX in a concentration-dependent manner. (B-D) F-PABA and 2-F-NB but not 2-F-NAP can rescue the inhibition of growth caused by SMX.

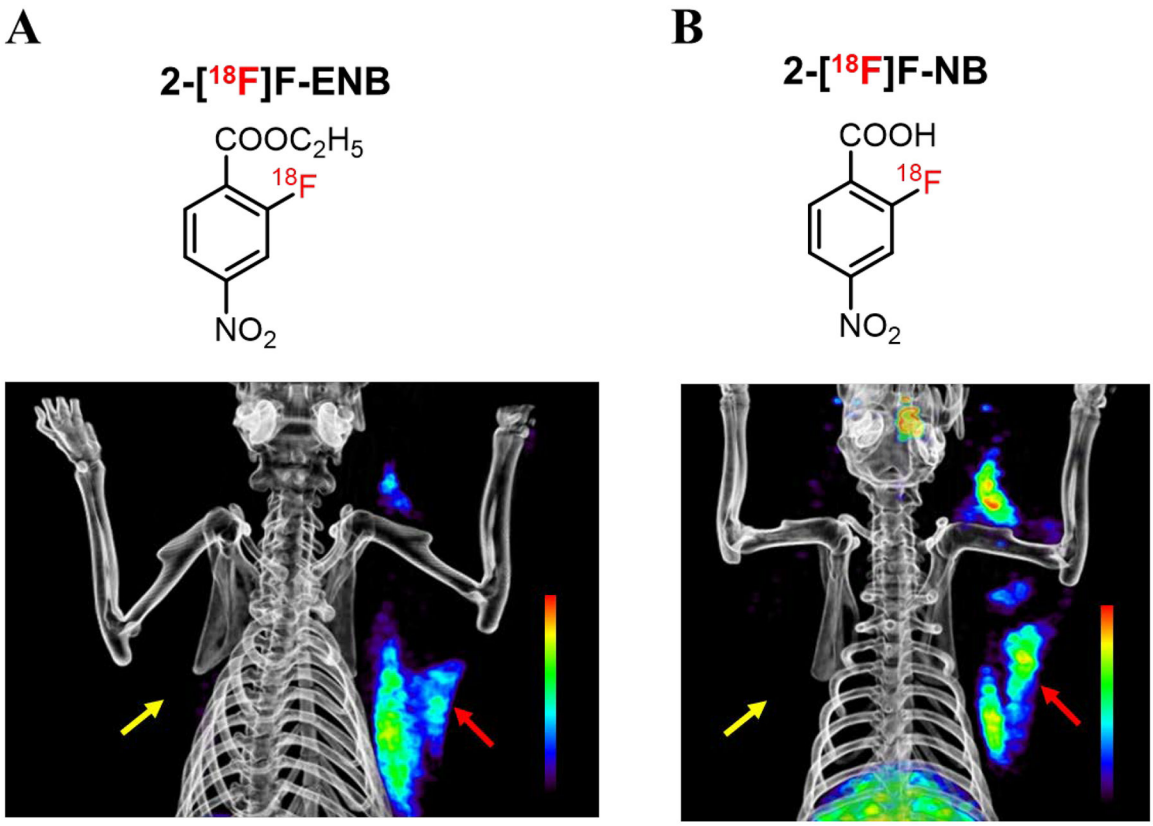

Figure 7. A comparison of PET imaging of the triceps infection/inflammation model with 2-[^{18}F]F-ENB (A) and 2-[^{18}F]F-NB (B).

Both radiotracers were shown to localize the *S. aureus* Xen 29 infection (red arrow) with no accumulation at the site of inflammation (yellow arrow), 3 h post injection of radiotracers.

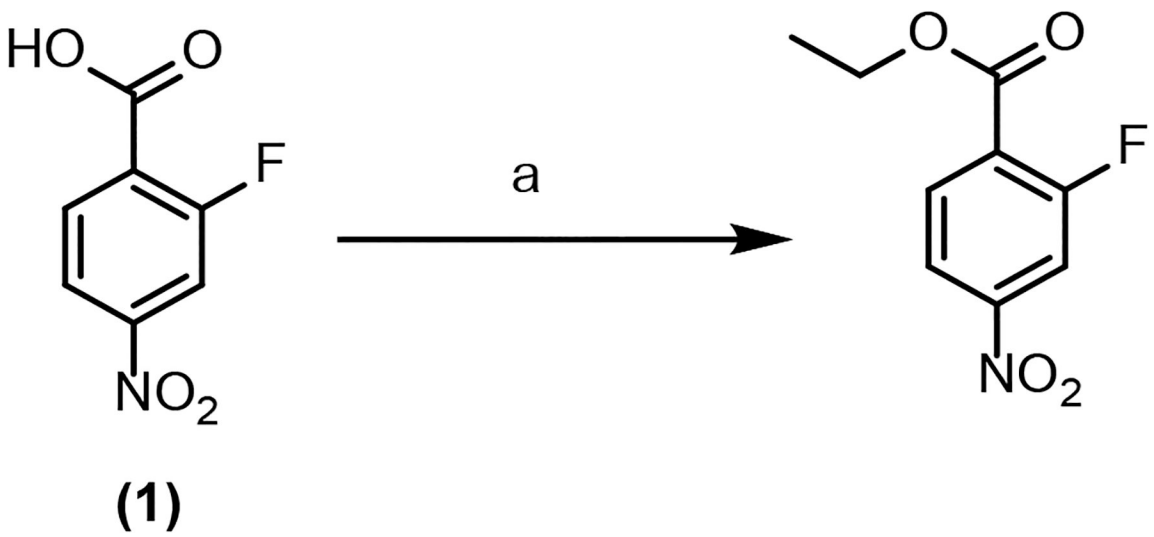

(1)

Scheme 1. Synthesis of ethyl 2-fluoro-4-nitrobenzoate

[a]Reagents and reaction conditions: (a) N-(3-Dimethylaminopropyl)-N′-ethylcarbodiimide hydrochloride (EDC/HCl), *N,N*-dimethylpyridin-4-amine (DMAP), dimethylformamide (DMF), dichloromethane (DCM), ice bath, 30 min; ethanol, r.t. overnight.

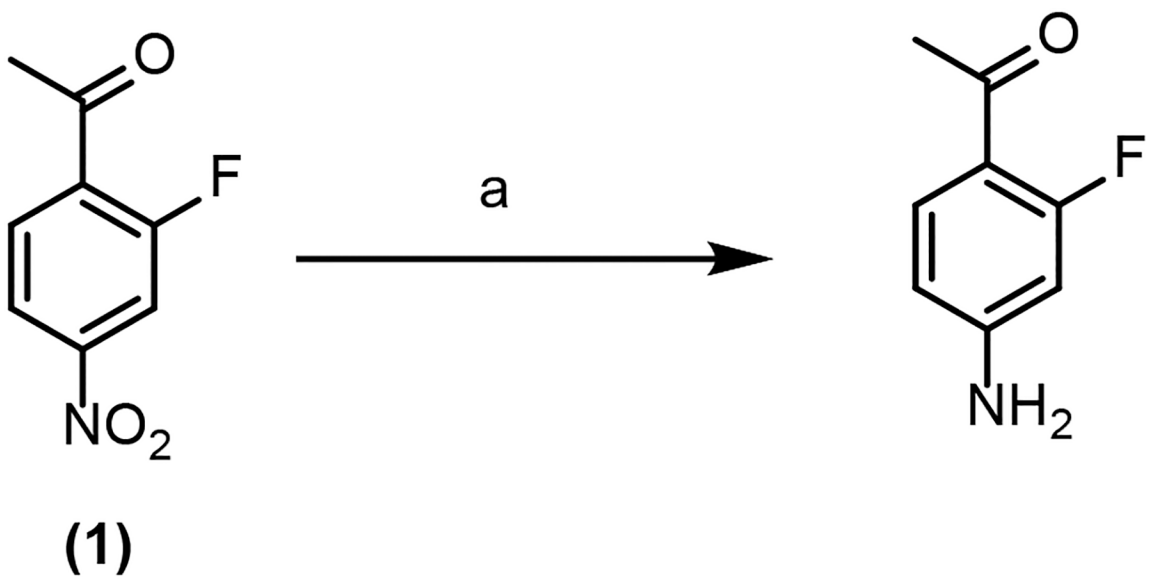

(1)

Scheme 2. Synthesis of 2-fluoro-4-aminoacetophenone

[a]Reagents and reaction conditions: (a) Zn powder, ammonium chloride, methanol and H_2O, 85 °C, 30 min.

Table 1.

Reduction of F-ENB and F-NB by NfsB[a]

Substrate	k_{cat} (s^{-1})	K_m (μM)	k_{cat}/K_m ($M^{-1}s^{-1}$)
2-F-ENB	16.1±1.7	28±8	5.7×10^5
2-F-NB	12.4±1.6	686±174	1.8×10^4

[a]Initial velocities were monitored at 340 nm at a fixed concentration of NADH (40 μM) and at varying concentrations of 2-F-ENB and 2-F-NB. Data were fit to the Michaelis–Menten equation.